THE JOURNAL OF PHYSICAL CHEMISTRY B

Article

pubs.acs.org/JPCB

Crystalline Polymorphs of [6,6]-Phenyl-C_{61}-butyric Acid *n*-Butyl Ester (PCBNB)

Soo-Hyung Choi,[†,‡] Christopher D. Liman,[‡,∥] Stephan Krämer,[∥] Michael L. Chabinyc,[‡,∥] and Edward J. Kramer*[,‡,§,∥,⊥]

[†]Department of Chemical Engineering, Hongik University, 121-791, Seoul, Korea

[‡]Mitsubishi Chemical Center for Advanced Materials, [§]Materials Research Laboratory, [∥]Materials Department, and [⊥]Department of Chemical Engineering, University of California, Santa Barbara, California 93106, United States

Supporting Information

ABSTRACT: The thermotropic behavior of [6,6]-phenyl-C_{61}-butyric acid *n*-butyl ester (PCBNB) in powder and thin film form was investigated using X-ray diffraction and transmission electron microscopy. Upon heating PCBNB powder above its glass-transition temperature, an amorphous-to-crystalline transition (i.e., cold crystallization) and a subsequent melting of these crystals were observed. A thin film of PCBNB was observed to order on a simple hexagonal lattice (HEX) with the *c* axis preferentially oriented normal to film at an annealing temperature of 180 °C but became disordered above 200 °C, consistent with the powder results. However, when annealed at 160 °C, the PCBNB thin film ordered on a superlattice of the HEX as indicated both by electron diffraction and high-angle annular dark field scanning TEM (HAADF-STEM) images. The formation of the HEX superlattice polymorph was independent of both solvent and substrate and could be formed both on heating from the amorphous as cast state and by cooling from the HEX structure formed at a higher temperature. HAADF-STEM shows that the superlattice corresponds to a regular deficiency of PCBNB molecules on every fifth $(1\ \bar{1}\ 0\ 0)$ plane of the HEX structure.

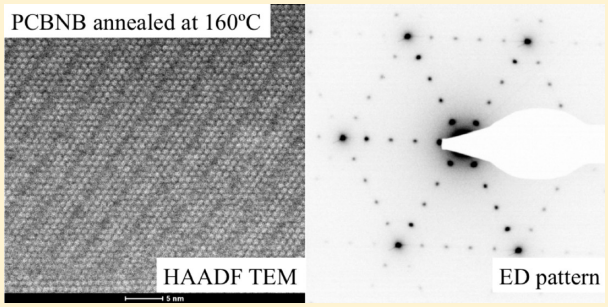

INTRODUCTION

Organic electronic devices have great potential for low-cost, flexible electronics because of the ability to use simple solution-processing methods for deposition of thin films.[1] One important challenge is to fabricate organic photovoltaics (OPVs) that achieve power-conversion efficiencies comparable to traditional inorganic photovoltaics.[2−5] Recent progress in solution-processed OPVs has improved power-conversion efficiency to ∼10%.[6] It has been widely accepted that the performance of OPVs is related to both molecular intrinsic electronic properties and morphological features such as phase separation and crystalline structure. Improved control of the interface between electron donors and acceptors and achievement of higher crystallinity is believed to be beneficial to improve power-conversion efficiency of OPVs.[7,8]

Fullerene derivatives are the most commonly employed electron acceptors in bulk heterojunction (BHJ) OPVs. In particular, [6,6]-phenyl-C_{61}-butyric acid methyl ester (PCBM) has been widely investigated because of its solubility in common solvents and its ability to phase separate into nanoscale domains for charge generation and extraction with most conjugated polymers.[9] Experiments have focused on the morphology of the blend (i.e., the phase separation of donor and acceptor) and the relationship to device performance.[2,10−15] Despite the significant progress on understanding the morphology of BHJs, less attention has been paid to the intrinsic phase behavior of the fullerene derivatives. The correlation between crystalline structure and electronic properties, such as the carrier mobility, can shed light on the way to achieve the best performance through optimization.[16] Despite recent computer simulations[17−19] and experiments,[13,20−23] the phase behavior of PCBM has not been fully resolved yet.

C_{60} molecules have been found to be ordered on a face-centered cubic (fcc) lattice in powder and thin films at room temperature.[24−26] However, the pendant group attached to C_{60} induces a significant change in the phase behavior relative to unsubstituted C_{60}. The crystalline structure of PCBM in both thin films and single crystals depends significantly on the preparation method such as choice of solvent, solvent evaporation rate, and annealing temperature.[13,20,22,23,27,28] Recently, Verploegen et al. investigated the temperature-dependent growth mechanism of PCBM crystals in thin films using grazing incidence X-ray scattering.[13] The density of nucleation sites depends on annealing temperature and determines growth mechanism and crystal orientation. The crystalline structure of PCBM in thin films and in single crystals upon thermal annealing was investigated systematically by Zheng et al.[22,23] They observed that the PCBM undergoes both

Received: August 23, 2012
Revised: October 10, 2012
Published: October 31, 2012

   dx.doi.org/10.1021/jp3083997 | J. Phys. Chem. B 2012, 116, 13568−13574

an amorphous-to-crystalline phase transition starting from an as-cast thin film (i.e., cold crystallization) and a crystalline-to-crystalline phase transformation upon heating further.

The present study focuses on the phase behavior of [6,6]-phenyl-C_{61}-butyric acid *n*-butyl ester (PCBNB) in powder and thin film form upon thermal annealing. PCBNB is structurally similar to PCBM but has a longer aliphatic tail (butyl vs methyl) (Figure 1), increasing its solubility in common solvents. The field effect mobility of PCBNB was reported to be an order of magnitude lower than that of PCBM,[29] and it has also been used as an acceptor in OPVs.[30−34] Interestingly, we observed that the small change in the molecular structure in PCBNB leads to remarkable difference in the phase behavior from PCBM, including a more sluggish crystallization on cooling, a decrease in melting temperature, and the presence of a stable superlattice phase. Because many BHJs are thermally annealed in the temperature range where these PCBNB crystal polymorphs are observed, these polymorphs and their formation are potentially of interest for OPV applications.

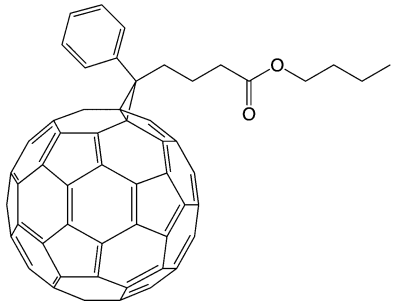

Figure 1. Molecular structure of [6,6]-phenyl-C_{61}-butyric acid *n*-butyl ester (PCBNB).

EXPERIMENTAL SECTION

Sample Preparation. PCBNB (Figure 1) was obtained from Mitsubishi Chemical and used as received. Poly(styrene sulfonate) and poly(3,4-ethylene dioxythiophene) (PEDOT:PSS, HC Starck) mixture in an aqueous solution was spin-coated on a silicon wafer covered by a 100−150 nm thick SiO_2 layer (Silicon Quest International), then annealed at 150 °C for 10 min. PCBNB in either toluene, chlorobenzene, or chloroform (ca. 12−15 mg/mL) was spin-coated on the PEDOT:PSS layer. Then, the thin film was annealed at the target temperature for more than 30 min, followed by rapid cooling to room temperature.

Differential Scanning Calorimetry. Differential scanning calorimetry (DSC) experiments were carried out with a TA Instruments Q2000 equipped with a nitrogen-cooling system. DSC samples were prepared by sealing ∼5 mg of material in aluminum T-zero pans (TA Instruments). To erase temperature history completely, we first heated samples to a temperature higher than the melting temperature and then cooled them down to room temperature at a rate of 10 °C/min. DSC scans were then obtained during heating of the sample at a ramp rate of 10 °C/min, which was followed by a cooling cycle at the same ramp rate.

Transmission Electron Microscope. Conventional transmission electron microscopy (TEM) was carried out on a FEI Tecnai G2 Sphera Microscope operating at 200 kV. For electron diffraction (ED) and imaging, the camera distance from the sample stage was calibrated with gold (Agar Scientific). The images and diffraction patterns were recorded on a Gatan Ultrascan CCD.

High-angle annular dark-field scanning TEM (HAADF-STEM) was performed on a FEI Titan operating at 300 kV. The convergence semiangle of the probe was set to 10 mrad. The HAADF detector (Fischione) inner and outer radii were 70 and 200 mrad, respectively (camera length: 100 mm). The extraction voltage of the HAADF detector was set to 4.4 kV at least 3 h before imaging to allow the diffracted intensity to stabilize.

Two types of TEM specimens were investigated: plane-view (top-down) samples and cross-sectioned samples. Top-down TEM specimens were prepared by submerging the thin film in a 5 vol % hydrofluoric acid solution to etch away the SiO_2 layer and then floating the resulting PCBNB thin film on the surface of deionized water. The floating thin film was picked up on a copper grid with a carbon support film (Ted Pella). Cross-sectioned specimens were prepared using a focused ion beam (FIB, FEI Helios 600 Dual Beam). Prior to sectioning, polystyrene and platinum layers were applied on top of the samples to protect the PCBNB thin film from ion beam damage. A Ga^+ ion beam was used to cut a thin hexahedron with a length of 20 μm and a thickness of ∼100 nm. Then, the cross-sectioned thin films were attached to an Omniprobe FIB lift-out grid (Ted Pella).

X-ray Diffractometer. X-ray Diffraction (XRD) measurements were performed using SmartLab (Rigaku) system with a wavelength of 1.54 Å (Cu Kα). The range of scattering angle θ between 3 and 50° was surveyed, which covers $2 < q < 34$ nm^{-1}, where q is a wave vector defined as $q = 4\pi\lambda^{-1} \sin(\theta/2)$. The acquired pattern was analyzed using DicVol software to estimate the peak positions and to index the diffraction peaks.[35]

RESULTS AND DISCUSSION

Powder Behavior. The thermotropic behavior of a PCBNB was investigated using DSC, as shown in Figure 2. The thermogram indicates that a glass transition (T_g) is observed at 85 °C, and two melting temperatures (T_m) were observed at 211 and 224 °C. A similar thermotropic trend has been

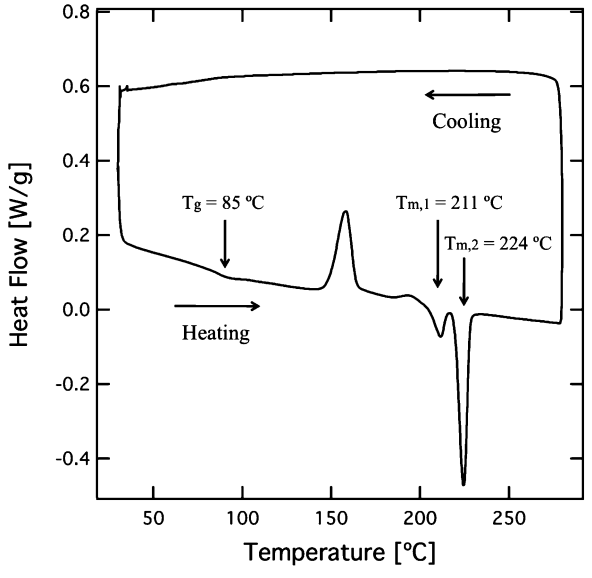

Figure 2. DSC thermogram of PCBNB powder obtained at a heating and cooling rate of 10 °C/min (endo down).

dx.doi.org/10.1021/jp3083997 | J. Phys. Chem. B 2012, 116, 13568−13574

observed with other fullerene derivatives, for example, PCBM in which a single T_m was reported as 285.2 °C.[22,36] Prior to the DSC measurement, the sample was heated to a high temperature (>250 °C) to erase the temperature history completely and then cooled to room temperature rapidly (i.e., 10 °C/min). The molecular mobility of PCBNB is such that crystallization is not observed upon reasonably rapid cooling (i.e., 10 °C/min), and molecules are frozen below T_g in the amorphous state. As a comparison, PCBM molecules show crystallization upon cooling at a rapid cooling rate of 10 °C/min.[22] PCBNB molecules are able to crystallize above T_g, which leads to exothermic behavior upon heating (i.e., cold crystallization). It is interesting that two melting peaks were observed, which might be attributed to two different crystal structures. Here it should be pointed out that relative to PCBM, three more methyl groups in the aliphatic ester induce a decrease in T_m by ~60 °C and slower crystallization upon cooling in comparison with PCBM.[22]

XRD was performed to identify the crystal structure of PCBNB below T_m. Figure 3 shows the XRD result obtained

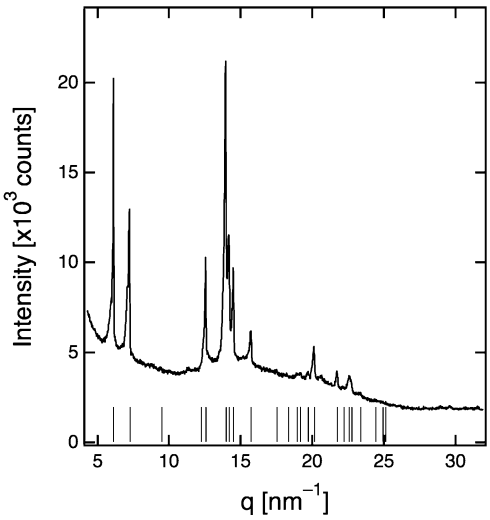

Figure 3. Powder X-ray patterns for PCBNB. The specimen was annealed at 180 °C for 30 min and quenched to room temperature. The sticks below the data are estimated peak position of simple hexagonal lattice (a = 10.01 Å, c = 10.29 Å).

from PCBNB powder, which was annealed at 180 °C for at least 30 min and quenched to room temperature quickly prior to the X-ray measurement.[37] The Bragg peaks were indexed on a primitive hexagonal lattice with lattice constants of a = 10.01 Å and c = 10.29 Å (i.e., c/a = 1.028). The estimated peak position is indicated by vertical bars in Figure 3. Higher order peaks such as [0 0 0 l] (where $l \neq 1$) as well as [1 0 $\bar{1}$ 1] are nearly absent, where q < 15 nm^{-1} due to limited resolution of lab source X-ray.

The simple hexagonal lattice with a = 10.01 Å and c = 10.29 Å is intriguing. A simple hexagonal structure has been observed for a fulleride solid ($C_{60}I_4$)[38] and has been theoretically proposed as one of the possible crystalline structures for PCBM[17] but not yet observed experimentally in other fullerenes to our knowledge. However, this simple hexagonal structure is not common in materials science, even though a few materials have been reported as having this crystalline structure.[39,40] Furthermore, the distances between PCBNB molecules along the a axis and c axis are 10.01 and 10.29 Å, respectively. Compared with C_{60} fullerene ordered onto an fcc lattice, these values indicate that the distance between PCBNB along the a axis is interestingly slightly smaller than C_{60} fullerene (= 10.08 Å),[24] and the pendant group of PCBNB is expected to be intercalated between (0 0 0 1) planes. This thermotropic behavior and crystalline structure of PCBNB powder provides a guideline to understand the behavior of PCBNB in a thin film.

PCBNB Thin Films. Thin films of PCBNB were prepared by annealing at target temperatures for at least 30 min and were subsequently cooled by placing the Si wafer on a metal plate at room temperature. We believe that the structural reorganization of PCBNB is so slow that the structure does not change upon reasonably rapid cooling. By referring to the powder DSC results, annealing temperatures for the thin films were chosen as 160, 180, and 200 °C, and the resulting thin films will be referred to as PCBNB 160, PCBNB 180, and PCBNB 200, respectively.

Figure 4 depicts the XRD patterns for both PCBNB 160 and PCBNB 180 thin films with (a) in-plane, (b) out-of-plane, and (c) reflectivity measurements. XRD results show that the PCBNB 160 and PCBNB 180 thin films have very similar structures. In Figure 4a,b, Bragg peaks are indexed using a simple hexagonal lattice, as observed for the powder sample (a = 10.01 Å and c = 10.29 Å). Bragg peaks of (0 0 0 l) are obtained in out-of-plane measurement that were not observed with powder XRD measurement. Therefore, PCBNB thin films prepared by thermal annealing are highly oriented such that the c axis is nearly perpendicular to the substrate.

In Figure 4c, Kiessig fringes in the low-q regime are attributed to the total thickness h of the PEDOT:PSS/PCBNB film (where q < 2 nm^{-1}), resulting in $h \approx$ 70 nm, and the Laue oscillations around the Bragg peak (where 5 < q < 7 nm^{-1}) are due to the thickness ~40 nm of the PCBNB crystallites. Considering the thickness of PEDOT:PSS layer (i.e., 30−40 nm under the spin-coating condition), this indicates that the PCBNB crystallites constitute the entire depth of the PCBNB film. This is confirmed by cross-sectional TEM images, as discussed later.

Figure 5 shows TEM bright-field images and the corresponding ED patterns from (a) PCBNB 160, (b) PCBNB 180, and (c) PCBNB 200 thin films. The PCBNB molecules become disordered at 200 °C, as indicated by the broad halo in ED pattern (Figure 5c). The DSC results on the PCBNB powder show that melting takes place above 200 °C at relatively fast heating rate (i.e., 10 °C/min), but the measured value in DSC is affected by kinetics of the melting transition. The fact that PCBNB 200 thin films are not crystalline after prolonged annealing and subsequent quenching is reasonably consistent with the DSC results on the PCBNB powder. We suspect that the dark spots observed in all samples in the bright-field image are contamination from the PEDOT:PSS below the PCBNB layer.[23]

PCBNB 180 thin films in Figure 5b show a single-crystal diffraction pattern indicating long-range hexagonal molecular ordering in-plane. For the ED pattern, the corresponding d spacings were determined to be 0.87, 0.50, 0.43, 0.33, and 0.29 nm in a decreasing order. (See Figure S1 in the Supporting Information.) It should be pointed out that PCBM thin films have also shown similar hexagonal ED patterns with a largest d spacing of ~0.85 nm.[21−23] Extended areas (tens of μm^2) of PCBNB 180 thin films show uniform in-plane orientation, which enables us to investigate the structure by tilted ED

dx.doi.org/10.1021/jp3083997 | J. Phys. Chem. B 2012, 116, 13568−13574

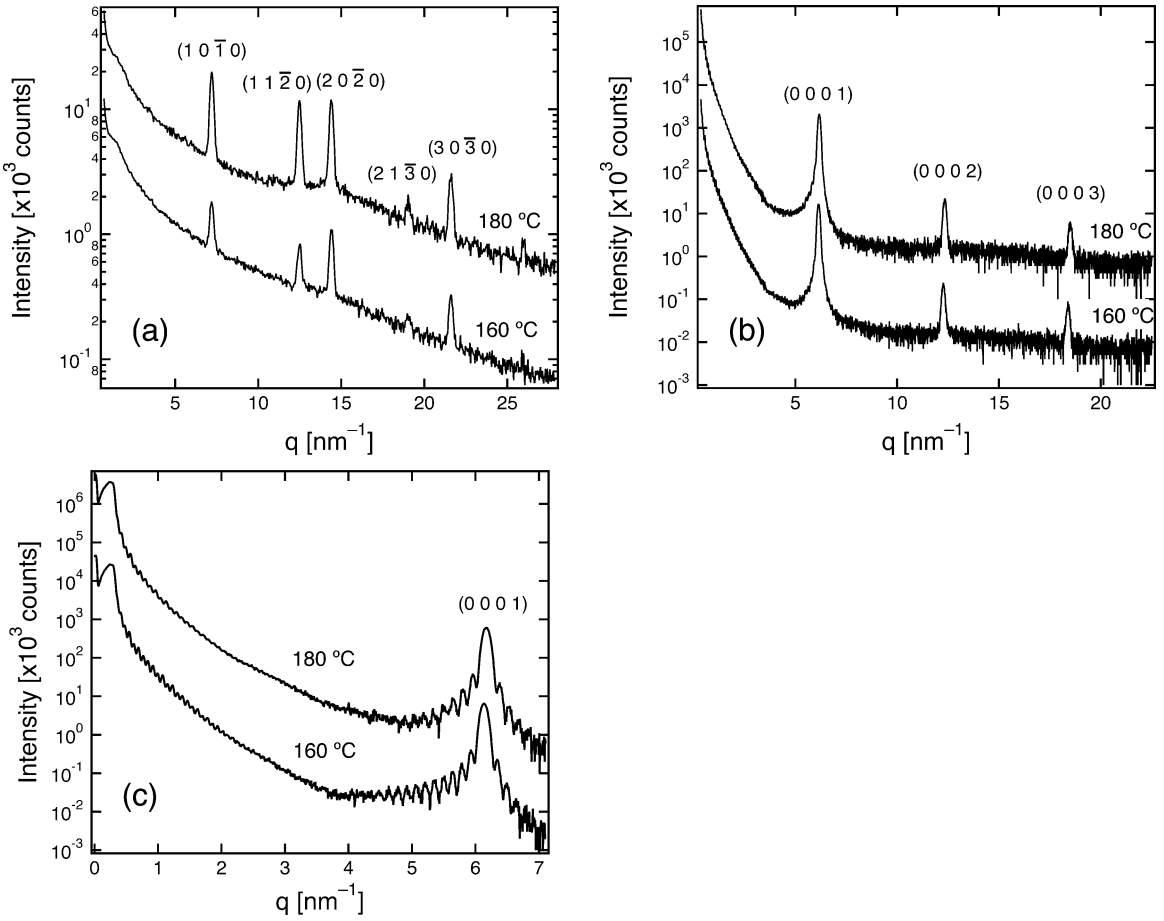

Figure 4. XRD patterns obtained for PCBNB 160 and 180 thin films: (a) in-plane measurement, (b) out-of-plane measurement, and (c) reflectivity measurement. The Bragg peaks are indexed using a simple hexagonal lattice (a = 10.01 Å and c = 10.29 Å) as shown in the figures. Data are shifted vertically for visibility.

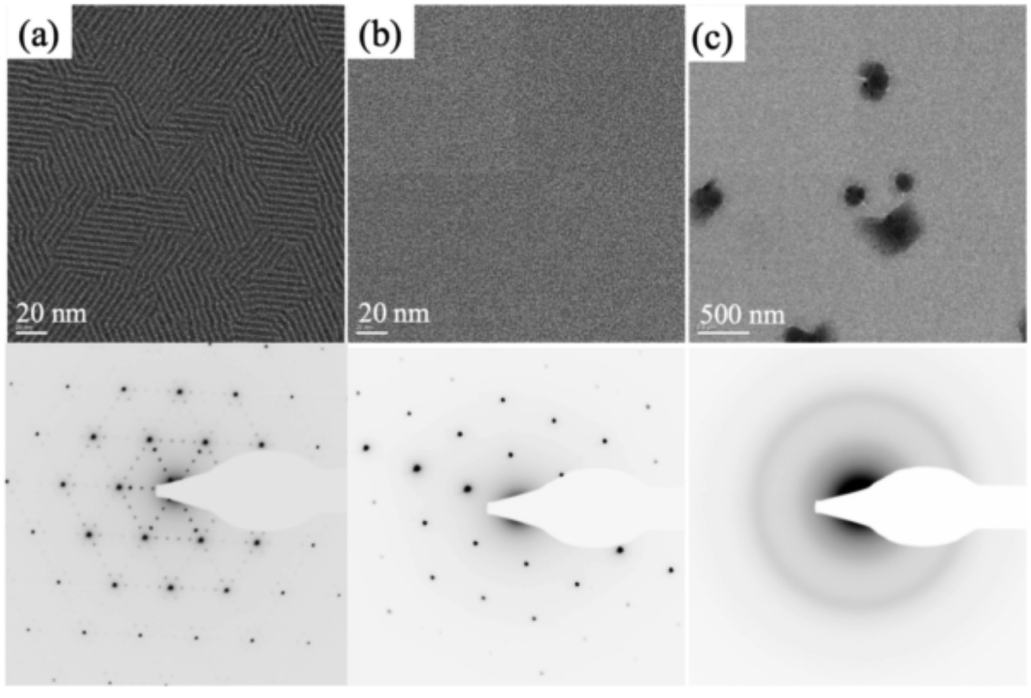

Figure 5. TEM bright-field image and corresponding electron diffraction patterns for PCBNB annealed at (a) 160, (b) 180, and (c) 200 °C.

dx.doi.org/10.1021/jp3083997 | J. Phys. Chem. B 2012, 116, 13568−13574

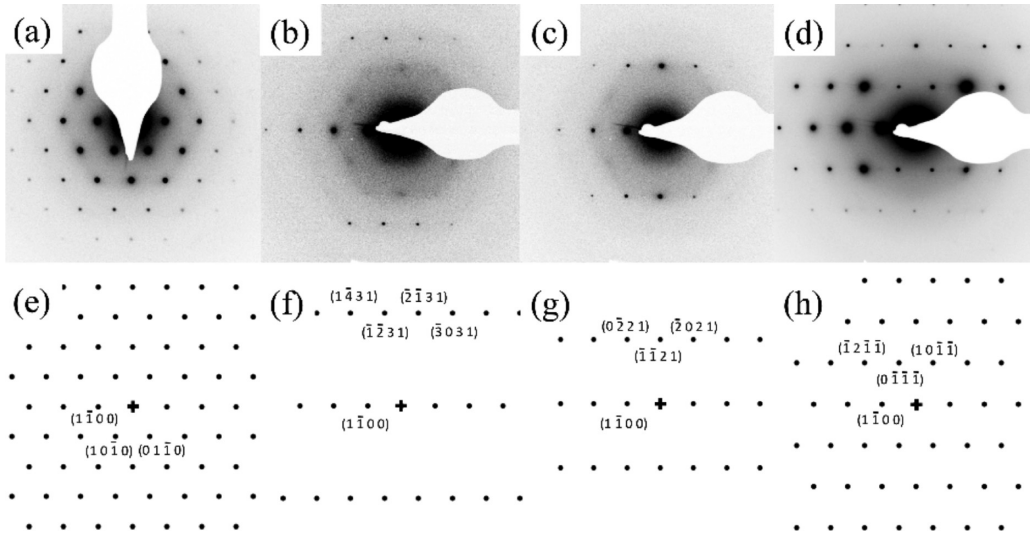

Figure 6. Rotation-tilt electron diffraction patterns of PCBNB thin films annealed at 180 °C with different rotation angles around (1 $\bar{1}$ 0 0) plane: (a) 0, (b) 17.5, (c) 25.5, and (d) 44.5°. The corresponding calculated electron diffraction patterns of simple hexagonal lattice (a = 10.01 Å and c = 10.29 Å) are displayed with the view vector of (e) [0 0 1] = [0 0 0 1], (f) [1 1 3] = [1 1 $\bar{2}$ 9], (g) [1 1 2] = [1 1 $\bar{2}$ 6], and (h) [1 1 1] = [1 1 $\bar{2}$ 3]. Calculated tilt angles are 0, 18.1, 26.1, and 44.4°, respectively. Beam center is indicated by cross marker.

measurements. Tilting the sample around identified crystallographic axes allows us to explore different sections of reciprocal space. Figure 6 displays the results of the rotation-tilt ED experiment on a PCBNB 180 thin film around the (1 $\bar{1}$ 0 0) axis in reciprocal space by angles of (a) 0, (b) 17.5, (c) 25.5, and (d) 44.5°. The hexagonal ED pattern can be obtained from crystals having both three-fold symmetry and six-fold symmetry. The fact that the diffraction patterns obtained by tilting at $+\theta$ and $-\theta$ are identical confirms the crystalline structure has six-fold symmetry. The ED patterns from tilted specimens can be reproduced with a simple hexagonal lattice with lattice constants of a = 10.01 Å and c = 10.29 Å. The zone axis of [1 1 $\bar{2}$ 9], [1 1 $\bar{2}$ 6], and [1 1 $\bar{2}$ 3] produces the same ED patterns observed from the tilt of the sample by 17.5, 25.5, and 44.5°, respectively. Furthermore, the experimental tilt angles are reasonably consistent with the calculated angles of 18.1, 26.1, and 44.4°, respectively. This shows good agreement with the XRD results that PCBNB thin films annealed at 180 °C are ordered on a simple hexagonal lattice and that the c axis is perpendicular to the substrate.

However, it is surprising that PCBNB 160 thin films show a superlattice structure, as indicated by the ED pattern and a domain texture seen in the bright-field image in Figure 5a. (A higher magnification image is available in the Supporting Information, Figure S2.) Four weaker diffraction peaks emerge between the strong diffraction peaks that appear in the PCBNB 180 thin films. The superlattice has a structure that repeats every five (1 $\bar{1}$ 0 0) planes. The direction of the superlattice rows is parallel to [1 1 $\bar{2}$ 0], and the angle between two superlattice rows is 60°. This superlattice structure from PCBNB 160 was not detected in the thin film XRD measurements mainly due to limited resolution of the lab source X-ray system.

The superlattice structure has been observed for PCBNB thin films spin coated from different solvents such as chloroform and chlorobenzene and then annealed at 160 °C for >30 min. In addition, this structure has been obtained from PCBNB thin films spin-coated both on PEDOT:PSS and on an SiO_2 layer. (Data are not shown.) Therefore, both solvent and substrate do not affect the formation of the superlattice structure. In addition to the thin film annealed at 160 °C after spin-casting, the superlattice structure was also observed from the thin films prepared by spin-casting, heating to 230 °C for 1 h, and annealed at 160 °C for 1 h (Supporting Information, Figure S3). Therefore the superlattice structure is the equilibrium PCBNB crystalline structure at 160 °C.

To obtain more detail about the crystalline structure of PCBNB, we performed high-angle annular dark-field scanning TEM (HAADF-STEM) on PCBNB 160 and PCBNB 180 thin films, as shown in Figure 7. HAADF images are formed from

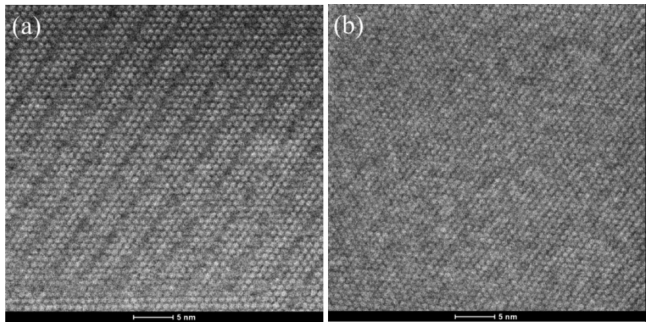

Figure 7. High-angle annular dark-field image (top-down view) for PCBNB thin films annealed at (a) 160 and (b) 180 °C. Scale bar indicates 5 nm. Bright circles in the HAADF images represent PCBNB C_{60} cages that are perfectly aligned along film normal and electron beam direction (film thickness ~40 nm).

electrons scattered with large scattering angles, resulting in images dominated by Z-contrast.[41] Heavier atoms scatter more electrons, leading to a brighter image in HAADF-STEM. Therefore, brighter circles of ~1 nm diameter in Figure 7 represent PCBNB C_{60} cages. Here it should be pointed out that PCBNB molecules are perfectly aligned in columns (i.e., AAAA... type) along the c axis (film normal) to produce the bright circles, which is consistent with the simple hexagonal structure.

dx.doi.org/10.1021/jp3083997 | J. Phys. Chem. B 2012, 116, 13568−13574

For the PCBNB 180 thin film (Figure 7b), PCBNB C_{60} cages are placed on a hexagonal lattice, consistent with the previous results. However, dark streaks were observed for the PCBNB 160 thin film (Figure 7a), which indicates a regular deficiency of PCBNB C_{60} cages in every fifth $(1\ \bar{1}\ 0\ 0)$ plane. Therefore, this spatially regular deficiency in C_{60} cages is the origin of the superlattice structure. Furthermore, we strongly suspect that a periodic preferential orientation of the pendant butyl ester group induces the regular deficiency.

Figure 8 displays (a) high-resolution bright-field image and (b) HAADF image of a cross-sectioned PCBNB thin film annealed at 160 °C. The specimen was prepared by focused ion beam sectioning. Polystyrene and platinum layers were applied to protect the PCBNB thin film from ion beam damage. The PCBNB film thickness is measured as 42 nm, and the c axis of the PCBNB crystalline structure is preferentially oriented perpendicular to the substrate throughout the entire film, which is consistent with the thin film X-ray reflectivity data (Figure 4c).

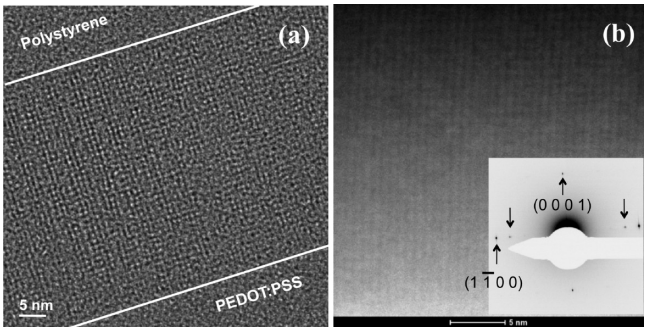

Figure 8. Cross-sectional PCBNB 160 thin film: (a) high-resolution bright-field image and (b) HAADF image. Lines indicate an upper and lower boundary of PCBNB. ED pattern corresponding to the view vector of $[1\ 1\ \bar{2}\ 0]$ is shown in the inset. Scale bar indicates 5 nm.

It is apparent that this projection produces two-fold symmetry where the $[1\ 1\ \bar{2}\ 0]$ is parallel to the electron beam. In the inset of Figure 8b, the ED pattern shows Bragg diffraction peaks from $(1\ \bar{1}\ 0\ 0)$ and $(0\ 0\ 0\ 1)$, which is consistent with simple hexagonal lattice of $c/a = 1.028$. Diffraction from the superlattice is also obtained at $q = 4/5 \times q_{(1\ \bar{1}\ 0\ 0)}$, as indicated by down-pointing arrows in the ED pattern. However, additional peaks are not observed in the out-of-plane direction (i.e., c axis). Therefore, only the in-plane structure perpendicular to the c axis shows the formation of a superlattice. (Note: This is also confirmed by GIWAXS results shown in the Supporting Information.)

On the basis of the ED patterns and HAADF images, we envision the superlattice structure formed by PCBNB thin film annealed at 160 °C illustrated in Figure 9. Twenty PCBNB molecules in simple hexagonal ordering with five C_{60} deficient sites provides a building block ($a' = b' = 50.05$ Å) that is tiled to allow the texture shown in Figure 5a. This structure explains that the angle between two superlattice rows is 60°, as shown in Figure 9 with red and green building blocks. Then, the layer is stacked on top of the others with $c' = 10.29$ Å. Note that we do not claim that the open circles are empty, only that the probability of occupancy of these sites by C_{60} cages is considerably <1. These sites may also contain a high concentration of butyl side chains.

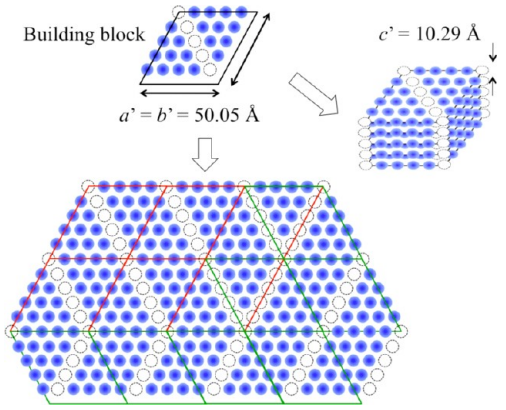

Figure 9. Hypothetical packing structure of PCBNB thin film annealed at 160 °C. Filled spheres represent PCBNB molecules, and blank spheres represent deficiency of the molecule. The building block ($a' = 50.05$ Å and $c' = 10.29$ Å) is composed of 20 PCBNB molecules ordered on simple hexagonal lattice (five of them are deficient), and tiling of the building block provides the angle between superlattice row2 of 60°. There are ~30 layers of PCBNB molecules in the 40 nm thick film.

CONCLUSION

In this work, the phase behavior of PCBNB molecules in both powders and thin films was investigated upon thermal annealing. Investigation of thermotropic behavior and crystalline structure of PCBNB powder provides guidance to understand the thin film behavior. In thin films, the PCBNB molecules are ordered on simple hexagonal lattice with the c axis perpendicular to the substrate when annealed at 180 °C below melting temperature. At the lower annealing temperature of 160 °C, superlattice formation with a basis of simple hexagonal ordering was observed, resulting from regular deficiency of PCBNB molecule along every fifth $(1\ \bar{1}\ 0\ 0)$ plane. The schematic phase behavior of PCBNB thin film is illustrated in Figure 10. These results are tentatively attributed to the orientation of the pendant group that is preferentially oriented at 160 °C but randomly oriented at 180 °C due to higher thermal energy. However, other explanations cannot be completely excluded, so further study is necessary. Nonetheless, it is clear that the simple addition of three more methylene groups in the ester chain produces a striking difference in the phase behavior of PCBNB relative to PCBM.

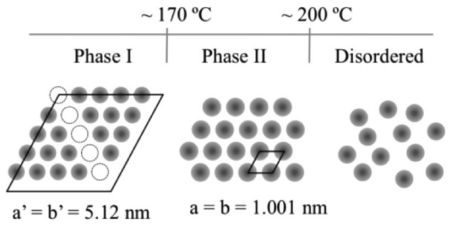

Figure 10. Temperature-dependent phase behavior of the PCBNB thin film. Dark spheres represent PCBNB molecules, and blank ones indicate deficiency of the molecules.

ASSOCIATED CONTENT

Supporting Information

Indexing the XRD peaks, azimuthally averaged electron diffraction profile for PCBNB thin film, high-resolution TEM bright field image and the corresponding electron diffraction

dx.doi.org/10.1021/jp3083997 | J. Phys. Chem. B 2012, 116, 13568−13574

pattern for PCBNB 160, superlattice structure observed after melting and cooling to 160 °C, TEM bright field image of PCBNB thin film, and grazing incidence wide-angle X-ray scattering (GIWAXS). This material is available free of charge via the Internet at http://pubs.acs.org.

AUTHOR INFORMATION

Corresponding Author

*E-mail: edkramer@mrl.ucsb.edu.

Notes

The authors declare no competing financial interest.

ACKNOWLEDGMENTS

This work was supported by Mitsubishi Chemical through the Mitsubishi Chemical Center for Advanced Materials at UCSB. We acknowledge the use of the Central Facilities of the Materials Research Laboratory (MRL) at UCSB, which is supported by the MRSEC Program of the NSF under award no. DMR-1121053. We thank Dr. Youli Li at MRL for assistance with XRD measurements.

REFERENCES

(1) Myers, J. D.; Xie, J. *Polym. Rev.* **2012**, *52*, 1−37.
(2) Deibel, C.; Dyakonov, V. *Rep. Prog. Phys.* **2010**, *73*, 096401.
(3) Slota, J. E.; He, X.; Huck, W. T. S. *Nano Today* **2011**, *5*, 231−242.
(4) Weickert, J.; Dunbar, R. B.; Hesse, H. C.; Wiedemann, W.; Schmidt-Mende, L. *Adv. Mater.* **2011**, *23*, 1810−1828.
(5) Li, G.; Yang, Y. *Nat. Photon.* **2012**, *6*, 153−161.
(6) www.nrel.gov/ncpv/images/efficiency_chart.jpg (accessed Oct 21, 2012).
(7) Peet, J.; Kim, J. Y.; Coates, N. E.; Ma, W. L.; Moses, D.; Heeger, A. J.; Bazan, G. C. *Nat. Mater.* **2007**, *6*, 497−500.
(8) Rogers, J. T.; Schmidt, K.; Toney, M. F.; Kramer, E. J.; Bazan, G. C. *Adv. Mater.* **2011**, *23*, 2284−2288.
(9) Hummelen, J. C.; Knight, B. W.; LePeq, F.; Wudl, F.; Yao, J.; Wilkins, C. L. *J. Org. Chem.* **1995**, *60*, 532−538.
(10) Hoppe, H.; Sariciftci, N. S. *J. Mater. Chem.* **2006**, *16*, 45−61.
(11) Yang, X.; Loos, J. *Macromolecules* **2007**, *40*, 1353−1362.
(12) Ruderer, M. A.; Müller-Buschbaum, P. *Soft Matter* **2011**, *7*, 5482−5493.
(13) Verploegen, E.; Mondal, R.; Bettinger, C. J.; Sok, S.; Toney, M. F.; Bao, Z. *Adv. Funct. Mater.* **2010**, *20*, 3519−3529.
(14) Beal, R. M.; Stavrinadis, A.; Warner, J. H.; Smith, J. M.; Assender, H. E.; Watt, A. A. R. *Macromolecules* **2010**, *43*, 2343−2348.
(15) Lilliu, S.; Agostinelli, T.; Verploegen, E.; Pires, E.; Hampton, M.; Al-Hashimi, M.; Heeney, M. J.; Toney, M. F.; Nelson, J.; Macdonald, J. E. *Macromol. Rapid Commun.* **2011**, *32*, 1454−1460.
(16) Choi, J.; Honda, T.; Seki, S.; Fukuzumi, S. *Chem. Commun.* **2011**, *47*, 11213−11215.
(17) Nápoles-Duarte, J. M.; Reyes-Reyes, M.; Ricardo-Chavez, J. L.; Garibay-Alonso, R.; López-Sandoval, R. *Phys. Rev. B* **2008**, *78*, 035425.
(18) Cheung, D. L.; Troisi, A. *J. Phy.s Chem.* **2010**, *114*, 20479−20488.
(19) MacKenzie, R. C. I.; Frost, J. M.; Nelson, J. *J. Chem. Phys.* **2010**, *132*, 064904.
(20) Rispens, M. T.; Meetsma, A.; Rittberger, R.; Brabec, C. J.; Sariciftci, N. S.; Hummelen, J. C. *Chem. Commun.* **2003**, 2116−2118.
(21) Yang, X.; van Duren, J. K. J.; Rispens, M. T.; Hummelen, J. C.; Janssen, R. A. J.; Michels, M. A. J.; Loos, J. *Adv. Mater.* **2004**, *16*, 802−806.
(22) Zheng, L.; Liu, J.; Ding, Y.; Han, Y. *J. Phys. Chem. B* **2011**, *115*, 8071−8077.
(23) Zheng, L.; Han, Y. *J. Phys. Chem. B* **2012**, *116*, 1598−1604.
(24) Dorset, D. L.; McCourt, M. P. *Acta Crystallogr.* **1994**, *A50*, 344−351.
(25) van Tendeloo, G.; van Heurck, C.; van Landuyt, J.; Amelinckx, S.; Verheijen, M. A.; van Loosdrecht, P. H. M.; Meijer, G. *J. Phys. Chem.* **1992**, *96*, 7424−7430.
(26) Elschner, C.; Levin, A. A.; Wilde, L.; Grenzer, J.; Schroer, C.; Leo, K.; Riede, M. *J. Appl. Crystallogr.* **2011**, *44*, 983−990.
(27) Swinnen, A.; Haeldermans, I.; vande Ven, M.; D'Haen, J.; Vanhoyland, G.; Aresu, S.; D'Olieslaeger, M.; Manca, J. *Adv. Funct. Mater.* **2006**, *16*, 760−765.
(28) Dabirian, R.; Feng, X.; Ortolani, L.; Liscio, A.; Morandi, V.; Müllen, K.; Samori, P.; Palermo, V. *Phys. Chem. Phys.* **2010**, *12*, 4473−4480.
(29) Morita, T.; Takashima, W.; Kaneto, K. *Jpn. J. Appl. Phys.* **2007**, *46*, L256−L258.
(30) Zheng, L.; Zhou, Q.; Deng, X.; Yuan, M.; Yu, G.; Cao, Y. *J. Phys. Chem. B* **2004**, *108*, 11921−11926.
(31) Sato, Y.; Niinomi, T.; Hashiguchi, M.; Matsuo, Y.; Nakamura, E. *Proc. SPIE* **2007**, *6656*, 66560U.
(32) Sato, Y.; Niinomi, T.; Abe, Y.; Matsuo., Y.; Nakamura, E. *Proc. SPIE* **2008**, *7052*, 70520J.
(33) Guide, M.; Dang, X.; Nguyen, T. *Adv. Mater.* **2011**, *23*, 2313−2319.
(34) Ku, S.; Liman, C. D.; Cochran, J. E.; Toney, M. F.; Chabinyc, M. L.; Hawker, C. J. *Adv. Mater.* **2011**, *23*, 2289−2293.
(35) Boultif, A.; Louër, D. *J. Appl. Crystallogr.* **2004**, *37*, 724−731.
(36) Chuard, T.; Deschenaux, R. *Helv. Chim. Acta* **1996**, *79*, 736−741.
(37) XRD profile from PCBNB powder annealed at 160 °C is nearly similar to that from 180 °C.
(38) Zhu, Q.; Cox, D. E.; Fischer, J. E.; Kniaz, K.; McGhie, A. R.; Zhou, O. *Nature* **1992**, *355*, 712−714.
(39) Zhang, J.; Sides, S.; Bates, F. S. *Macromolecules* **2012**, *45*, 256−265.
(40) Fornasini, M. L.; Manfrinetti, P.; Mazzone, D. *J. Solid State Chem.* **2006**, *179*, 2012−2019.
(41) Loos, J.; Sourty, E.; Lu, K.; de With, G.; v. Bavel, S. *Macromolecules* **2009**, *42*, 2581−2586.